Keratin/alginate hybrid hydrogels filled with halloysite clay nanotubes for protective treatment of human hair

Giuseppe Cavallaro,[a,b,*] Maria Rita Caruso,[a] Stefana Milioto,[a,b] Rawil Fakhrullin,[c] Giuseppe Lazzara[a,b]

[a]*Dipartimento di Fisica e Chimica, Università degli Studi di Palermo, Viale delle Scienze, pad. 17, 90128 Palermo, Italy.* giuseppe.cavallaro@unipa.it

[b]*Consorzio Interuniversitario Nazionale per la Scienza e Tecnologia dei Materiali, INSTM, Via G. Giusti, 9, I-50121 Firenze, Italy.*

[c]*Institute of Fundamental Medicine and Biology Kazan Federal University, Kreml uramı 18, Kazan, Republic of Tatarstan, 420008, Russian Federation*

KEY WORDS. Halloysite nanotubes, Keratin, Alginate, Hydrogel, Composite, Hair treatment

Abstract

Keratin/alginate hydrogels filled with halloysite nanotubes (HNTs) have been tested for the protective coating of human hair. Preliminary studies have been conducted on the aqueous colloidal systems and the corresponding hydrogels obtained by using Ca^{2+} ions as crosslinkers. Firstly, we have investigated the colloidal properties of keratin/alginate/HNTs dispersions to explore the specific interactions occurring between the biomacromolecules and the nanotubes. Then, the rheological properties of the hydrogels have been studied highlighting that the keratin/alginate interactions and the subsequent addition of HNTs facilitate the biopolymer crosslinking. Finally, human hair samples have been treated with the hydrogel systems by the dipping procedure. The protection efficiency of the hydrogels has been evaluated by studying the tensile properties of hair fibers exposed to UV irradiation.

In conclusion, keratin/alginate hydrogel filled with halloysite represents a promising formulation for hair protective treatments due to the peculiar structural and rheological characteristics.

1. Introduction

In recent years, hydrogels based on biocompatible macromolecules have been extensively investigated for numerous applications, including soft robotics [1–3], tissue engineering [4,5] and biomedicine [6,7]. Among biomacromolecules, alginate is a hydrophilic polysaccharide that can be employed for the fabrication of functional hydrogel systems though both ionic and covalent crosslinking of its polymeric chains [8]. The ionic gelation of alginate can be achieved by the addition of divalent cations (such as Ca^{2+}, Sr^{2+} and Ba^{2+}) in alginate aqueous solutions [9]. It should be noted that the kinetics of the crosslinking process is affected by the alginate molecular weight as well by the pH of the aqueous solvent generating the formation of hydrogels with tunable viscoelastic characteristics [10]. Alginate hydrogels presents some limitations in terms of low shear modulus [11] and poor cell adhesion [12] that prevent their use for bioprinting purposes. The mechanical properties of the alginate-based hydrogels can be improved by the incorporation of fillers, such as silica [11], clay nanoparticles [13,14], cellulose and polylactic nanofibers [15,16]. The filling of alginate hydrogels with molybdenum dioxide nanosheets generated composite gels systems suitable as wearable sensors due to their tunable photomechanical properties and excellent conductivity [3]. 3D printable hydrogels were obtained by embedding halloysite clay nanotubes within the alginate network [13,17,18].

Alternatively, alginate can be combined with another polymer that can drive to obtain hybrid hydrogels with enhanced mechanical strength because of specific supramolecular interactions occurring between the macromolecules [19,20]. Within this, the combination of alginate and gelatin is proper for the preparation of blended hydrogels with high mechanical performances and suitable cell adhesion for 3D bioprinting [12,21]. Alginate combined with carboxymethyl cellulose drives to obtain hydrogel systems useful for drug delivery applications [22]. Composite hydrogels based on alginate and modified chitosan exhibited excellent swelling and antimicrobial properties [23]. Hyaluronic acid can be employed as additive of alginate hydrogel to generate hybrid systems with improved shear-thinning behavior and injectability [24]. Numerous studies [5,25] evidenced that the

addition of proteins can favor the cell attachment of alginate hydrogels, which presents enhanced biocompatibility and availability helpful for medical and pharmaceutical purposes. In this context, keratin is a promising protein due to its fibrous structure related to its large content of cysteine residues [26]. As example, the human hair keratin possesses 18 wt% of cysteine [27]. Literature reports that keratin and alginate can be mixed to produce hybrid hydrogels with excellent mechanical stability and biocompatibility suitable for tissue engineering regeneration [5,28]. Due its high bioactivity, the addition of keratin within the alginate network could enhance the biomedical and cosmetic applications of the biopolymeric hydrogel [5].

In this paper, keratin/alginate network was filled with halloysite nanotubes (HNTs) to fabricate composite hydrogels appropriate as cosmetic formulations for hair protection. Halloysite represents a versatile nanofiller for biopolymeric matrices in both gel and solid phases driving to the formation of nanocomposite materials proper for several applications, including food packaging [29–32] and remediation [33–35]. Due to its low toxicity, halloysite can be used as nanocarrier of drugs [36–40], reinforcing agent of scaffolds for tissue engineering [41–43] and filler for hair protective coating [39,44–48]. Moreover, HNTs are efficient supports for heterogeneous catalysis because of their large specific surface and their tunable surface chemical composition, which allows to control the active sites of the reactions [49–56]. As shown in literature, halloysite/protein hybrids are effective in numerous applications, including enzyme immobilization [57], dye removal [58], sustained release of bioactive molecules [59,60] and bone tissue engineering [61]. In our previous work [44], we proved that keratin/halloysite aqueous mixtures can be employed for the protective treatment of human hair on dependence of pH, which affect the specific interactions between the protein and the HNTs surfaces. Here, we developed a novel protocol for the hair treatment by confining keratin and halloysite within an alginate gel matrix, which can guarantee a broad range of applications within hair care formulations because of the peculiar viscoelastic characteristics.

2. **Experimental**

2.1. Materials

Halloysite nanotubes (HNTs) were provided by Imerys Ceramics from Matauri Bay deposit. Hydrolyzed keratin was a gift from Kelisema srl. Sodium hydroxide (NaOH), hydrochloric acid (HCl) and sodium alginate are Sigma products. Calcium chloride dihydrate ($CaCl_2 \cdot 2H_2O$) is from Merck. Human hair samples were procured from a healthy Caucasian female, 30 years old with no special treatment. The hair type was straight, while its color was black.

2.2. Preparation of keratin/alginate mixtures in water

Preliminarily to the preparation of the mixtures, we separately prepared keratin and alginate solutions to investigate the colloidal properties of the pristine biopolymer and protein in water. Keratin solutions were analyzed at variable pH values (from 1.5 to 9.5), while alginate solutions were studied only at pH $\geq$ 5 because the biopolymer cannot be solubilized under strong acidic conditions [62]. The solutions were prepared by magnetically stirring for 2 hours at 25 °C. Both the keratin and alginate concentrations were kept constant at 0.1 wt%. The pH conditions of the aqueous medium were controlled by the addition of appropriate amounts of NaOH or HCl (0.1 mol dm^{-3}) dropwise. The aqueous colloidal characteristics of keratin were compared with those obtained in our previous work [44].

Afterwards, the keratin/alginate aqueous mixtures with variable composition were prepared by mixing variable amounts of keratin and alginate solutions at pH = 7. The mixtures were magnetically stirred for 2 hours at 25 °C. The keratin/alginate mass ratio ($R_{K:A}$) was varied from 0 to 3.

2.3 Preparation of halloysite dispersions in keratin/alginate aqueous mixture

Variable amounts of halloysite nanotubes were added to the keratin/alginate aqueous mixture (pH = 7) with $R_{K:A}$ = 1. The obtained dispersions were sonicated for 15 minutes and magnetically stirred

overnight at 25 °C. The mass ratio between halloysite and keratin + alginate ($R_{H/(K+A)}$) was systematically changed up to 0.2.

2.4 Preparation of the keratin/alginate hydrogels

The hydrogels were obtained by solubilizing both keratin and alginate in an aqueous solution of $CaCl_2 \cdot 2H_2O$ (0.1 mol dm^{-3}), which acts as crosslinker for the biopolymer. The alginate concentration was kept constant at 2 wt%, while the keratin concentrations were systematically varied at 0.5, 1 and 2 wt%. On this basis, we prepared keratin/alginate hybrid hydrogels with variable $R_{K:A}$ (0.25, 0.5 and 1). Similarly to the preparation of the corresponding aqueous mixtures, the stabilization of the hybrid hydrogels was achieved by magnetically stirring for 2 hours at 25 °C. For comparison, hydrogel formed by pristine alginate was prepared.

2.5 Preparation of the keratin/alginate hydrogels filled with halloysite nanotubes

Halloysite nanotubes were added to the keratin/alginate hydrogels. The HNTs concentration was fixed at 1 wt%. The stabilization of HNTs was obtained by sonication for 15 minutes and subsequent stirring overnight at 25 °C. For comparison, HNTs were filled to alginate based hydrogel. The preparation of the keratin/alginate hydrogel used for the hair treatment is sketched in Figure 1a.

2.4 Human hair treatment by immersion within the hybrid hydrogels

The hybrid hydrogels were tested for the treatment of human hair by using the immersion protocol presented in Figure 1b. In detail, the hair samples were immersed within the keratin/alginate hydrogel ($R_{K:A}$ = 1 and pH = 7) filled with HNTs (1 wt%). For comparison, the hair immersion procedure was conducted using alginate and keratin/alginate ($R_{K:A}$ = 1) hydrogels without halloysite. In general, the immersion time of the hair within the hydrogel systems was kept constant at 60 minutes. Afterwards, the hair segments were quickly washed with water for three times and then, dried at 25 °C. Finally,

the treated hair samples were stored in controlled conditions in terms of relative humidity (75 ± 1%) and temperature (25 ± 0.1 °C).

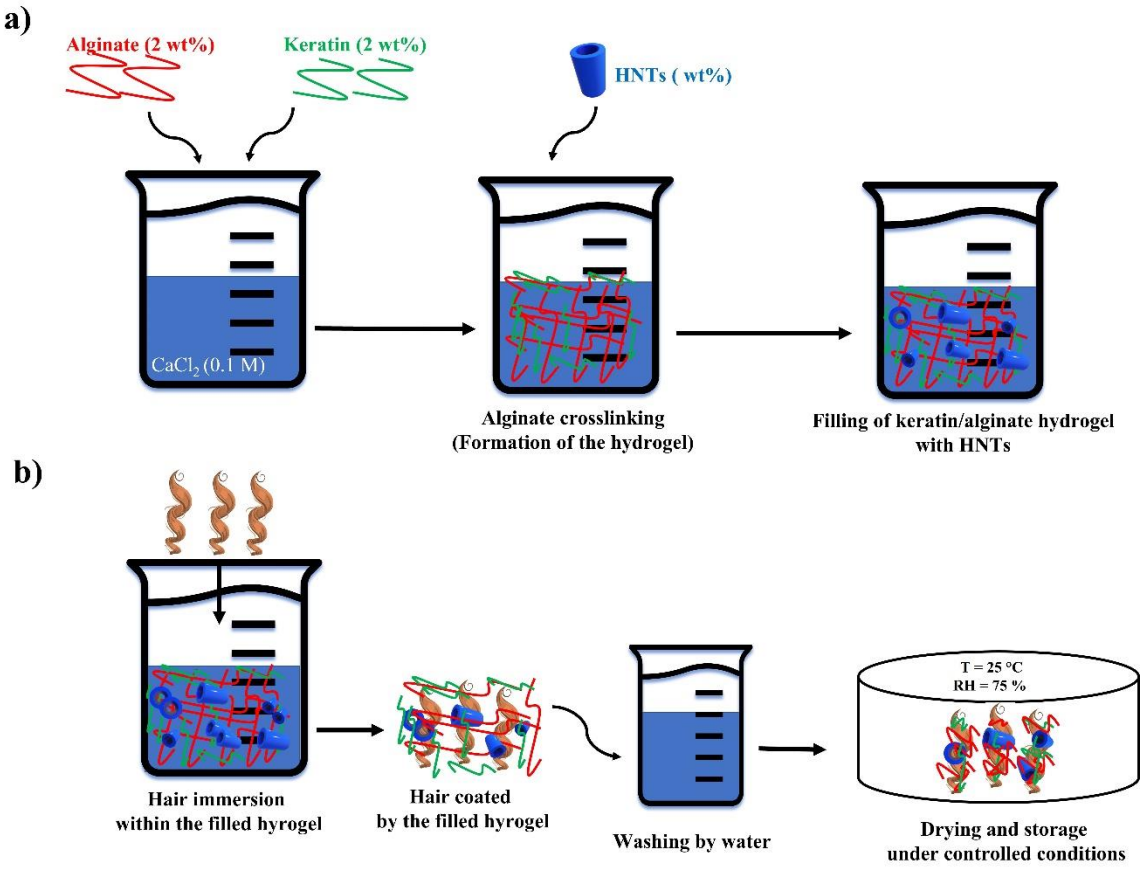

Figure 1. Schematic representation of the preparation of keratin/alginate/HNTs hydrogel (a) and the hair treatment protocol (b).

2.5. Aging of hair samples by UV irradiation exposure

Aging tests on untreated and treated hair samples were performed by their exposure to UV-A radiation. The irradiation was kept at 500 Wm^{-2}, while the aging times were set at 3 and 7 days. After their UV aging, hair fibers treated by keratin/alginate hydrogel filled with HNTs were also exposed to a flux of hot air for 60 seconds by using a commercial hair dryer kept at 15 cm. During the drying, the temperature of the hair surface was 45 °C.

2.6 Methods

2.6.1 Dynamic Light Scattering (DLS) and ζ-potential

Dynamic Light Scattering (DLS) and ζ-potential experiments were carried out by means of Zetasizer Nano-ZS (Malvern Instruments). Both DLS and ζ-potential measurements were conducted on alginate and keratin aqueous solutions at variable pH and keratin/alginate mixtures in water at pH = 7. Moreover, the experiments were performed on stable colloidal systems obtained by the addition of halloysite nanotubes to the keratin/alginate aqueous mixture ($R_{K:A}$ = 1). Details on the concentrations of halloysite, keratin and alginate of the investigated colloids are presented in the paragraphs 2.2 and 2.3. All the analyses were conducted at 25 °C.

As concerns DLS analyses, the wavelength and the scattering angle were set at 632.8 nm and 173°, respectively, while the field-time curves were analysed through ILT.

2.6.2 Rheological analysis

The rheological properties of the aqueous colloidal systems (2 wt% alginate solution, keratin/alginate mixtures, and keratin/alginate/HNTs dispersions) and the corresponding hydrogels were investigated by using a rheometer (Discovery HR-1, TA Instruments) equipped with a parallel plate (40 mm diameter and 1 mm gap size). The temperature was set at 25 °C for all experiments. The concentrations of alginate, keratin, HNTs and $CaCl_2 \cdot 2H_2O$ (the crosslinker) of the hydrogels are reported in the paragraph 2.4.

We performed shear-viscosity tests in a flow ramp mode by increasing the shear rate from 0.1 to 1000 s^{-1} within 60 s. The viscosity vs shear rate trends were fitted by using the Cross equation, which revealed successful for the data analysis of alginate solutions [63].

Moreover, we investigated the viscoelastic properties of the colloids and the hydrogels by dynamical oscillatory frequency sweep, which was carried out with a constant strain amplitude (1%) and a variable angular frequency (from 0.01 to 100 rad s^{-1}).

2.6.3 Dynamic Mechanical Analysis (DMA)

Dynamic Mechanical Analysis (DMA) was carried out on untreated and treated hair samples by using the DMA Q800 (TA Instruments). Tensile tests were conducted under a controlled force ramp (0.02 N min^{-1}) at 25.0 ± 0.1 °C. Based on the analysis of the stress vs strain curves, we determined the stress values at yield and breaking points, the Young modulus and the ultimate elongation.

2.6.4 Scanning Electron Microscopy (SEM)

Morphological investigations of treated hair samples were conducted by using a SEM microscope (Desktop SEM Phenom PRO X PHENOM). The energy of beam ranged between 4.8 and 20.5 kV. As concerns SEM analyses, each sample was preliminarily coated with gold to avoid charging effects under an electron beam.

3. Results and discussion

3.1 Effect of pH on the surface charge of keratin and alginate

Firstly, we investigated the influence of pH on the surface charge of both keratin and alginate dispersed in water. As shown in Figure 1S (see Supplementary Material), the ζ potential of keratin decreases with the pH due to the specific ionization equilibria of the functional groups of protein.

The fitting analysis of the ζ potential vs pH trend by an exponential decay function allowed us to estimate that the isoelectric point of keratin corresponds to pH = 3.8, which is close to that observed in our previous study [44]. We observed that keratin possess a positive ζ potential for pH < 3.8 reaching the largest value of +17.6 mV at pH = 1.5. Above the isoelectric point, the protein is negative with a minimum value of -37.4 at pH = 9.5.

As concerns alginate, the ζ potential experiments were conducted only at pH ≥ 5 being that the biopolymer is poorly soluble in water under acidic conditions [62]. According to its anionic characteristics due to the presence of the carboxylate groups, alginate possess a negative charge within the investigated pH interval. Specifically, the ζ potential of the biopolymer ranges between -

48.3 and -60.2 mV at pH equals to 5.0 and 9.5, respectively. Similar results were observed in literature [64].

The obtained data were useful to interpret the colloidal properties of keratin/alginate mixtures before and after the addition of halloysite nanotubes.

3.2 ζ potential and dynamic behavior of keratin/alginate mixtures in water

We explored the surface charge and the aqueous dynamic behavior of keratin/alginate mixtures with variable composition. These studies were carried out at pH = 7, where both keratin and alginate present negative ζ potential values (-22.8 and -59.8 mV, respectively).

Figure 2 shows the dependence of the ζ potential on the keratin/alginate mass ratio ($R_{K:A}$).

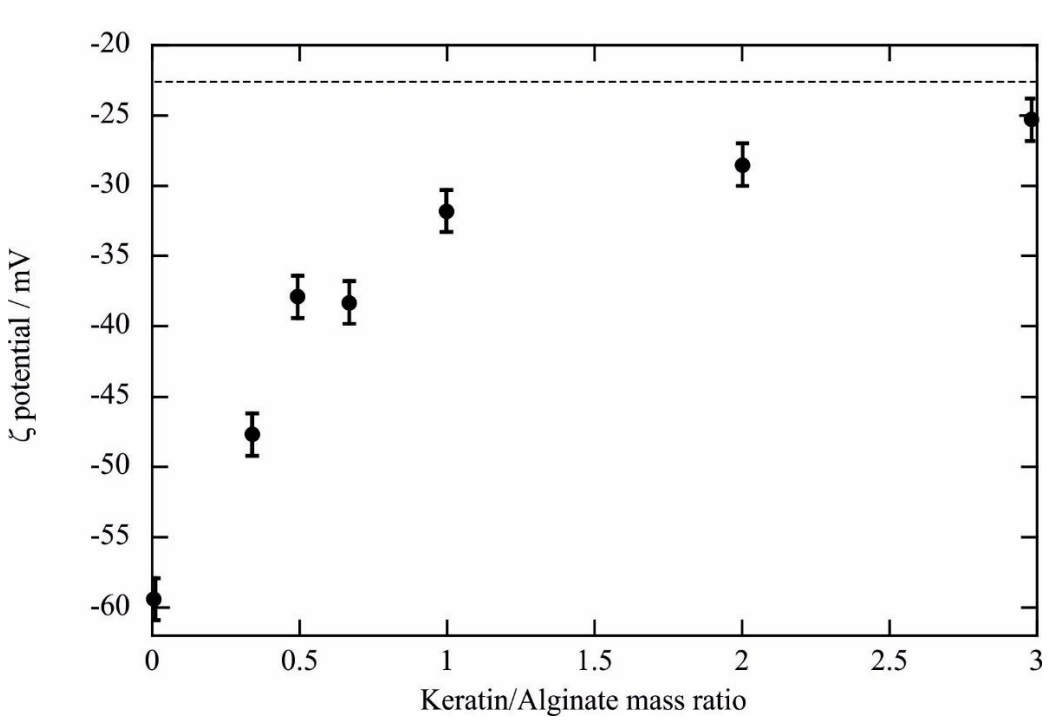

Fig. 2. ζ potential of keratin/alginate aqueous mixtures at pH = 7 as a function of the mass ratio between the protein and the biopolymer. The dashed line represents the ζ potential (-22.8 mV) of the keratin aqueous solution at pH = 7.

As expected, the surface charge of the mixtures is negative within the whole composition interval. In particular, the ζ potential ranges between those of the pristine components. We observed that the ζ potential vs $R_{K:A}$ profile shows an exponential increasing trend. Namely, the ζ potential becomes less

negative by increasing the keratin amount in the mixture. It should be noted that the ζ potential variations cannot be explained by considering a simple additive effect of keratin on the surface charge of alginate. We detected that the absolute values of the experimental ζ potential are lower compared with those calculated by using the rule of mixtures for all the investigated mixtures (see Supplementary Material) evidencing that specific supramolecular interactions occur between alginate and keratin. Additional information on the colloidal and structural characteristics of the keratin/alginate hybrids were determined by DLS measurements. All the autocorrelation curves can be described by monoexponential decay functions, which provided the aqueous diffusion coefficients of the keratin/alginate complexes. Based on the Stockes Einstein equation, we calculated the corresponding hydrodynamic diameters (see Supplementary Material). We detected that the hydrodynamic diameters of the keratin/alginate mixtures are not significantly altered compared to those of pure keratin and alginate. Namely, the aqueous diffusion characteristics of the complexes are similar to those of pristine keratin and alginate. On this basis, we can state that the keratin/alginate interactions do not induce the formation of large aggregates that could enhance the sedimentation of the biomacromolecules.

3.3 ζ potential and dynamic behavior of halloysite dispersed in keratin/alginate aqueous mixtures

We studied the ζ potential of halloysite nanotubes dispersed in keratin/alginate mixtures under neutral pH conditions (Figure 3). These experiments were conducted by systematically changing the HNTs concentration, while the keratin/alginate was fixed at 1.

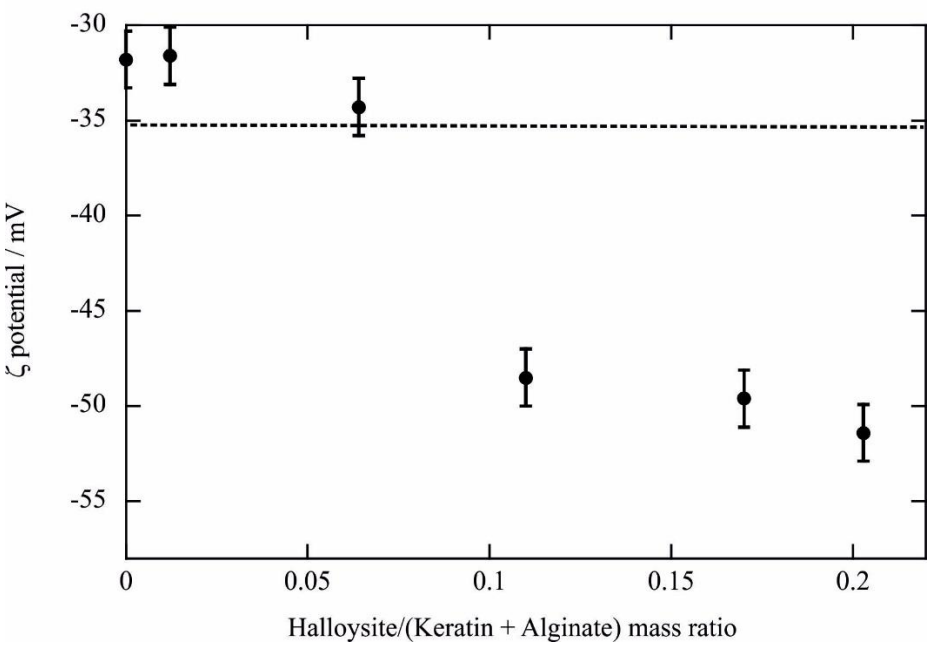

Fig. 3. ζ potential of halloysite dispersions in keratin/alginate mixtures at pH = 7 as a function of their composition. Both alginate and keratin concentrations were fixed at 0.1 wt%, while the halloysite content was systematically varied. The dashed line represents the ζ potential of pure halloysite in water at pH = 7.

As shown in Figure 3, the ζ potential of halloysite is negative for all the investigated dispersions, which possess variable composition in terms of mass ratio between HNTs and total amounts of both biomacromolecules ($R_{H/(K+A)}$). We observed that the ζ potential vs $R_{H/(K+A)}$ profile exhibits a sigmoidal decreasing trend that could be attributed to the adsorption of the keratin/alginate complex onto the HNTs surface. Specifically, the interactions are driven by electrostatic attractions between the HNTs inner surface (positive at pH = 7) and the keratin/alginate hybrid, which is negatively charged as demonstrated by its ζ potential (-31.8 mV). It should be noted that the ζ potential variations are negligible for $R_{H/(K+A)} > 0.1$, which corresponds to the composition at the saturation point. Namely, the ζ potential data highlighted that the HNTs inner surface is saturated by the keratin/alginate complex once the mass of the keratin/alginate complex is 10 times larger than that of halloysite. Similar results were observed for the adsorption of keratin onto halloysite nanotubes [44]. Interestingly, halloysite saturated by keratin/alginate possesses a lower ζ potential (ca. -50 mV) with respect to that of pristine HNTs (-35.0 mV). These results agree with the neutralization of the HNTs positive charges due to the specific attractive interactions between the keratin/alginate

complex and the halloysite inner surface. This consideration is supported by literature, which reports similar effects for the adsorption of anionic species (proteins, surfactants, biopolymers) onto halloysite nanotubes [65].

DLS measurements evidenced that the adsorption of keratin/alginate at the saturation point induces a small decrease of the HNTs hydrodynamic diameter. In particular, we determined hydrodynamic diameters of 520 ± 61 and 615 ± 70 for saturated and pristine nanotubes, respectively. On this basis, we can assert that HNTs mobility in water is slightly enhanced by the interactions with the keratin/alginate complex. This effect can be related to the increase of the net negative charge of HNTs evidenced by ζ potential data (Figure 3). Remarkably, DLS measurements highlighted that the adsorption of the biomacromolecules does not promote the aggregation of the nanotubes. The latter could indicate that the keratin/alginate complex is mostly confined within the HNTs lumen avoiding the hydrophobic interactions between the polypeptide and polymeric chains.

3.4 Rheological properties: influence of the biopolymer crosslinking on alginate/keratin/HNTs dispersions

Rheological measurements were conducted to investigate the actual formation of hydrogels after the addition of calcium chloride in the aqueous colloidal systems. According to the rheological data, we explored the mechanism of alginate crosslinking in the presence of keratin and halloysite nanotubes. Specifically, the keratin/alginate and keratin/alginate/HNTs systems (before and after the $CaCl_2$ addition) were studied by shear flow and frequency sweeps experiments to determine their viscosity characteristics and their rheological moduli, respectively. For comparison, the mentioned experiments were performed on the colloid and hydrogel based on pristine alginate.

3.4.1 Simple shear flow (steady measurements)

Figure 4 shows the influence of the $CaCl_2$ addition on the flow curves of the investigated colloidal systems (alginate, keratin/alginate and keratin/alginate/HNTs). As a general result, the viscosity

(η) decreases with the shear rate ($\dot{\gamma}$) indicating that all the samples behave like Non-Newtonian fluids. A more quantitative analysis of the η vs $\dot{\gamma}$ trends was conducted using the Cross fit model, which can be expressed by the following equation

$$\eta = \eta_\infty + (\eta_0 - \eta_\infty)/(1+(\alpha \cdot \dot{\gamma})^m) \quad (1)$$

where η_0 and η_∞ are the asymptotic viscosity values for low and high shear rate, α represents the relaxation time, and m is a dimensionless parameter related to the degree of dependence of η on $\dot{\gamma}$ in the shear–thinning region. Specifically, m equals to 0 and 1 can be attributed to Newtonian and plastic fluids, respectively, while m ranging between 0 and 1 reflects non-Newtonian pseudoplastic characteristics. According to literature [66,67], we assumed $\eta_\infty = 0$ being that the Newtonian plateaus at large velocities were not observed in the experimental η vs $\dot{\gamma}$ trends. This assumption was valid for the fitting analysis of flow curves of both polysaccharides solutions and polysaccharides/laponite clay dispersions [66].

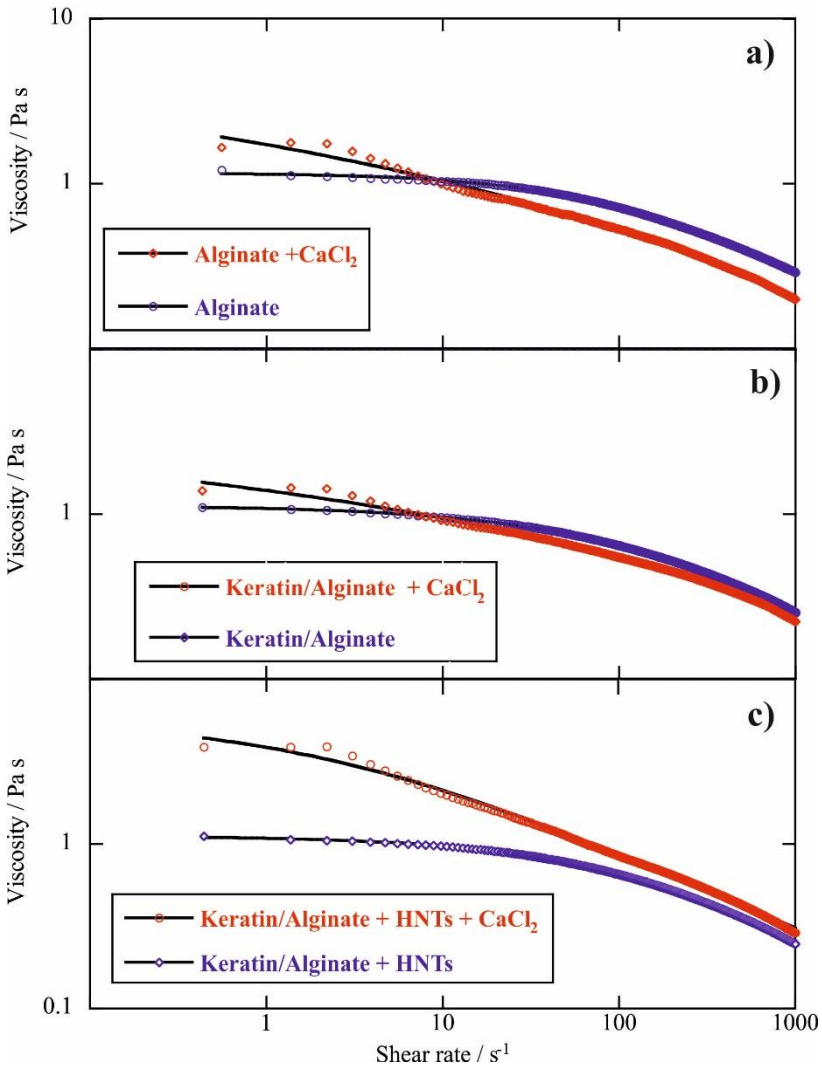

Fig. 4. Flow curves (shear viscosity as a function of shear rate) for alginate (a), keratin/alginate (b) and keratin/alginate + HNTs (c) before and after the addition of calcium chloride dihydrate. The black lines represent the fitting according to the Cross model (equation 1).

As evidenced in Figure 4, the Cross model was suitable for the data fitting analysis of both colloids and the corresponding hydrogels. The obtained parameters for all the samples are presented in Table 1.

Table 1. Fitting parameters obtained from the analysis of the flow curves based on Cross model.

Colloidal system	**η_0 / Pa·s**	**α / s**	**m**
	Colloidal system (before $CaCl_2$ addition)		
Alginate	1.164 ± 0.001	$(6.08 \pm 0.02) \cdot 10^{-3}$	0.759 ± 0.002
Keratin/Alginate ($R_{K:A} = 1$)	1.1261 ± 0.0007	$(5.660 \pm 0.019) \cdot 10^{-3}$	0.6268 ± 0.0011
Keratin/Alginate ($R_{K:A} = 1$) + HNTs	1.1186 ± 0.0006	$(5.622 \pm 0.009) \cdot 10^{-3}$	0.6677 ± 0.0010
	Hydrogel (after $CaCl_2$ addition)		
Alginate	4.5 ± 0.4	3.7 ± 0.8	0.286 ± 0.011
Keratin/Alginate ($R_{K:A} = 1$)	4.0 ± 0.4	4.2 ± 0.6	0.175 ± 0.014
Keratin/Alginate ($R_{K:A} = 1$) + HNTs	5.95 ± 0.11	0.32 ± 0.02	0.529 ± 0.007

In general, we observed that η_0 is enhanced after the $CaCl_2$ addition in agreement with the hydrogel formation due to the alginate crosslinking caused by calcium ions. On this basis, we can state that the presence of both keratin and halloysite does not prevent the hydrogel formation. As concerns the exponential parameter m, we estimated values lower than 1 for both colloids and hydrogels confirming their rheological behavior as non-Newtonian pseudoplastic fluids. Regarding the colloidal systems, both keratin and halloysite induced a slight m decrease proving that the shear-thinning behavior of alginate solution was reduced. Similar effects were detected for alginate/laponite aqueous dispersions [66]. The obtained data are consistent with literature, which reports that polymer aqueous solutions possess m values of ca. 0.66 [63]. As a general result, the hydrogels exhibited lower m values compared with the corresponding colloids. Among the hydrogel systems, we determined the largest m value for keratin/alginate/HNTs evidencing that the halloysite addition enhanced the pseudoplastic behavior of keratin/alginate hydrogel. Accordingly, it is reported that the presence of halloysite nanotubes enhances the shear thinning behavior of alginate crosslinked by calcium ions [13]. Due to the reduction of the mobility of polymeric chains, the hydrogels possess α values larger compared to those of the corresponding colloidal systems. Interestingly, the addition of calcium ions induced α increases by ca. 3 orders of magnitude in both alginate and keratin/alginate

systems, while α was enhanced by ca. 2 orders of magnitude in keratin/alginate/HNTs dispersions. These results indicate that the relaxation time of the crosslinked alginate is not significantly influenced by its interactions with keratin, while the filling of halloysite nanotubes within the keratin/alginate structure determined a reliable reduction of the mobility of biopolymeric chains. Namely, the rupture of the linkages in the keratin/alginate hydrogel is favored by the addition of halloysite nanotubes. As reported for alginate/HNTs hydrogels [18], clay nanotubes can limit the diffusion of the polymeric chains during shear altering the rheological characteristics of the gel systems.

The reciprocal of the relaxation time α allowed us to estimate the critical shear rate (γ^*), which is related to the transition from Newtonian to non-Newtonian behavior. As concerns the colloids, we determined γ^* values equal to 164, 178 and 177 s^{-1} for alginate, keratin/alginate and keratin/alginate/HNTs, respectively. As expected, the crosslinking of alginate produced the γ^* reduction indicating the shinning behavior was facilitated in the hydrogels. The interactions with keratin did not determine significant γ^* variations. In particular, we estimated γ^* of 0.27 ± 0.06 and 0.24 ± 0.01 s^{-1} for alginate and keratin/alginate, respectively. In contrast, HNTs generated a significant increase of the critical shear rate ($\gamma^* = 3.11 \pm 0.19$ s^{-1}).

3.4.2 Frequency sweeps experiments

Figure 5 compares the rheological moduli as a function of the angular frequency for alginate solution before (a) and after (b) the addition of calcium chloride.

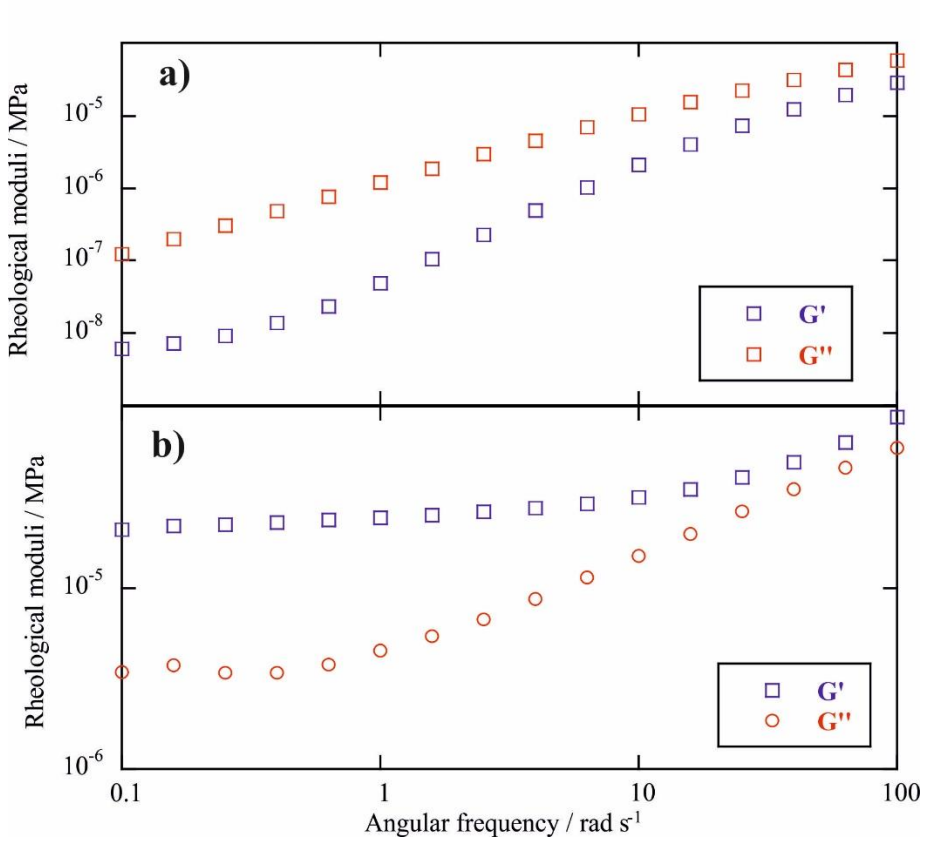

Fig. 5. Storage (G') and loss (G'') moduli as functions of the angular frequency for alginate solution before (a) and after (b) the addition of $CaCl_2$.

As a general result, the loss modulus (G'') is larger than the storage modulus (G') for alginate prior to its crosslinking by calcium ions (Figure 6a). These results indicate that the viscous component is predominant in agreement with the liquid-like behavior of the alginate solution [11].

The addition of calcium chloride generated an inversion of rheological moduli (G' > G'' within the whole angular frequency range), which reflect the variation of the viscoelastic properties of alginate. As expected for hydrogel system, the elastic component became predominant due to the crosslinking of the biopolymeric chains. Similar findings were detected on 2 wt% alginate solution after the $CaSO_4$ addition [11].

Then, we investigated the viscoelastic properties of keratin/alginate hydrogels with variable composition (Figure 6).

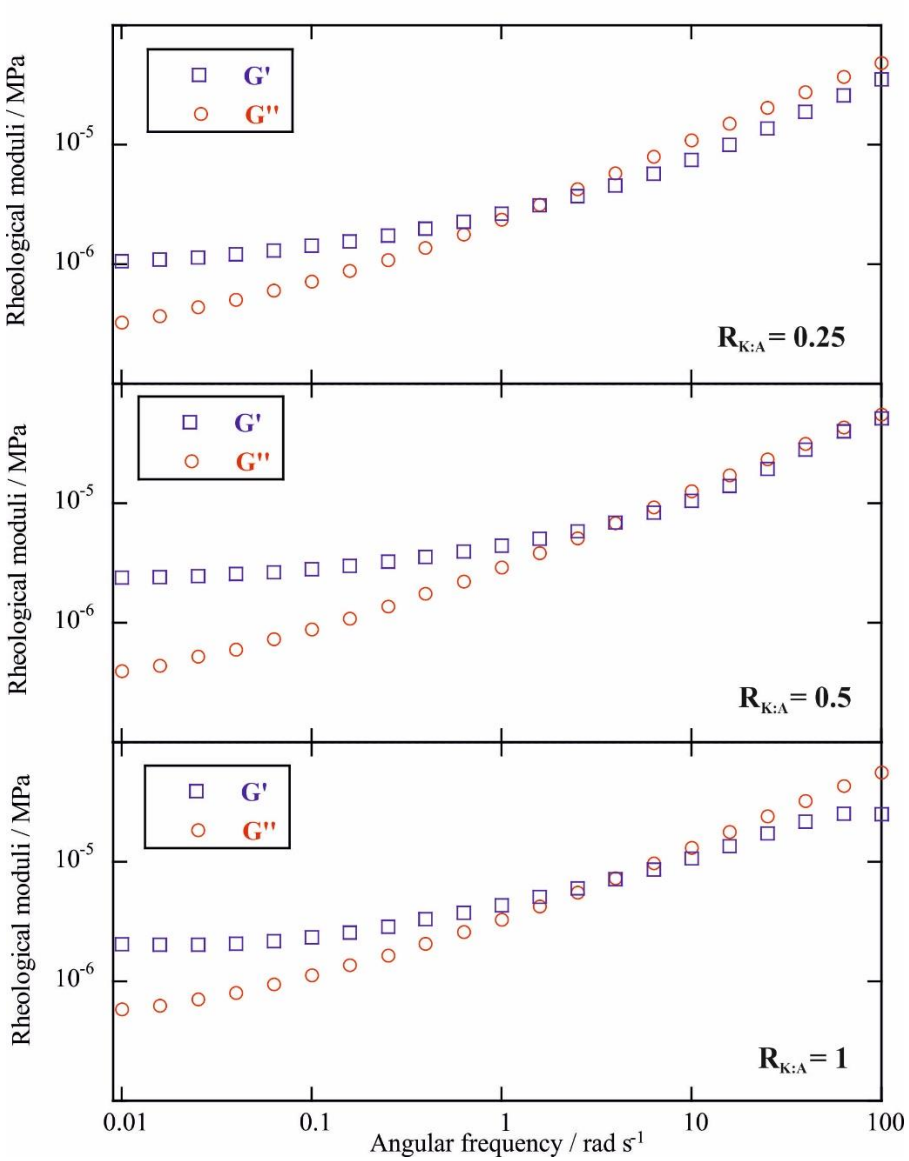

Fig. 6. Storage (G') and loss (G'') moduli as functions of the angular frequency for keratin/alginate hydrogels (after the $CaCl_2$ addition) with variable composition. The alginate concentration was fixed at 2 wt%, while the keratin concentration was systematically changed.

In general, we observed a crossing point between the G' and G'' curves indicating that the alginate crosslinking in the hybrid hydrogels is a reversible process. The angular frequency (ω^*) at the crossing point is related to variations on the rheological behavior of the composite hydrogels. Namely, the elastic part of the keratin/alginate hydrogels is predominant (G' > G'') for $\omega < \omega^*$ because the long-range rearrangements are slow. Oppositely, the composite hydrogels behave like a fluid (G'' > G') for $\omega > \omega^*$ indicating that short-range rearrangements are fast. Similar results were observed for aqueous suspensions of sodium alginate and montmorillonite clay [68]. As reported elsewhere for

polysaccharides based gels [9], we can determine the terminal relaxation time of keratin/alginate hydrogels by the inverse of the angular frequency at the crossover point of the rheological moduli. As shown in Table 2, the crossing point between G' and G'' moduli are shifted to higher frequencies by increasing the keratin content. Accordingly, the $R_{K:A}$ enhancement generates a reduction of the terminal relaxation time in the hybrid hydrogels. Specifically, we estimated terminal relaxation times ranging between 1.78 and 3.96 s for $R_{K:A}$ equals to 1 and 0.25, respectively.

Table 2. Frequency at the crossover point and terminal relaxation time of alginate in the composite hydrogels

Hydrogel	Crossover frequency / Hz	Terminal relaxation time / s
Keratin/Alginate ($R_{K:A}$ = 0.25)	0.252	3.96
Keratin/Alginate ($R_{K:A}$ = 0.5)	0.400	2.50
Keratin/Alginate ($R_{K:A}$ = 1)	0.560	1.78
Keratin/Alginate ($R_{K:A}$ = 0.25) + HNTs	n.d.	n.d.
Keratin/Alginate ($R_{K:A}$ = 0.5) + HNTs	6.34	0.058
Keratin/Alginate ($R_{K:A}$ = 1) + HNTs	0.676	1.48

As displayed in Figure 5, the hydrogel based on pure alginate does not show any crossover point between the rheological moduli demonstrating that the corresponding terminal relaxation time is > 628 s or < 0.0628 s. This consideration is consistent with previous studies on alginate crosslinked with several bivalent cations [9].

Furthermore, frequency sweeps experiments were conducted on keratin/alginate hydrogels filled with halloysite nanotubes. The obtained rheological data are displayed in Figure 7.

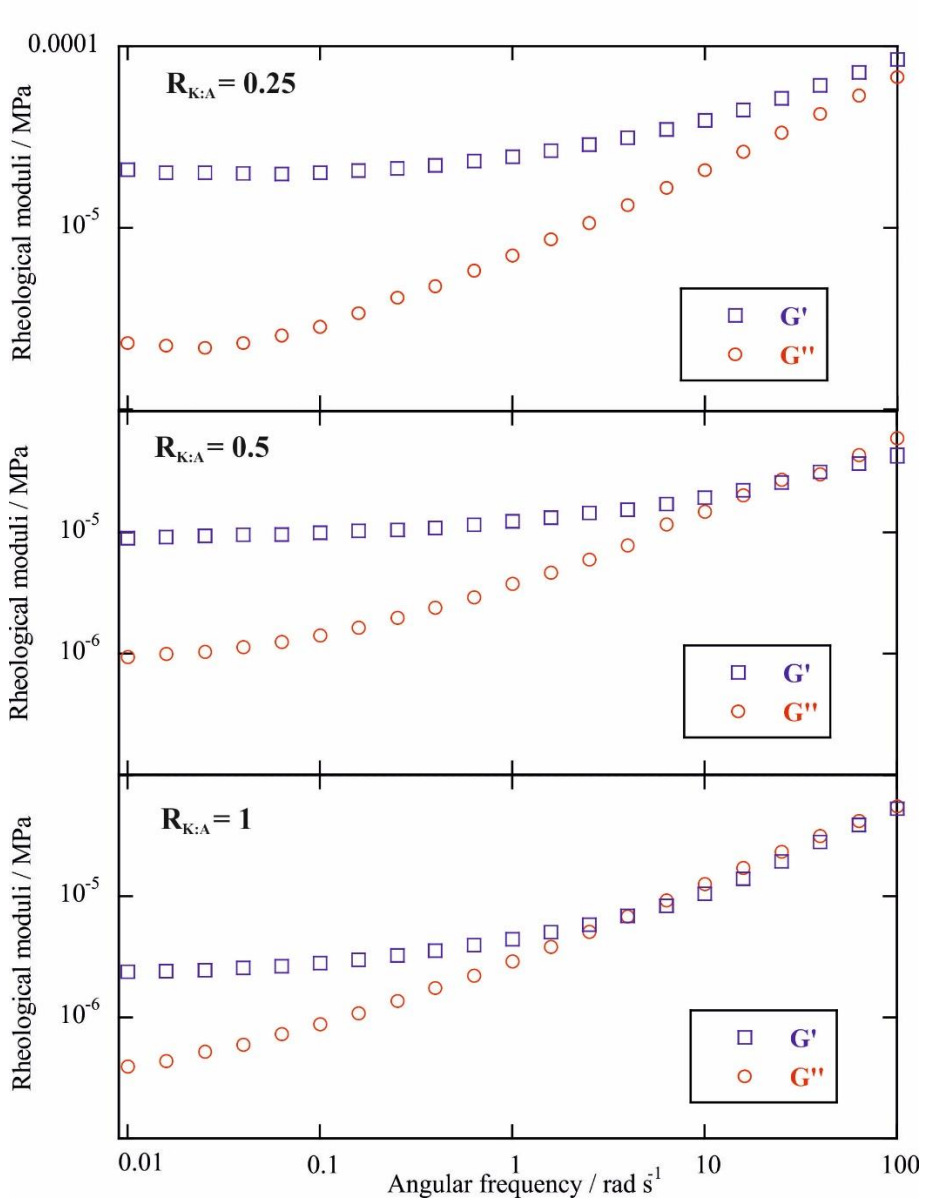

Fig. 7. Storage (G') and loss (G'') moduli as functions of the angular frequency for keratin/alginate hydrogels (after the $CaCl_2$ addition) filled with halloysite nanotubes with variable composition. The alginate and the halloysite concentrations were fixed at 2 and 1 wt%, respectively, while the keratin concentration was systematically changed.

We detected that the influence of halloysite on the rheological behavior of keratin/alginate hydrogels depends on their composition. In particular, we observed the crossover point between G' and G'' functions for $R_{K:A}$ equal to 0.5 and 1 allowing us to estimate the terminal relaxation times of the hydrogels filled with HNTs. Contrarily, this estimation was not conducted for $R_{K:A} = 0.25$ being that the elastic component is predominant (G' > G'') within the whole ω interval.

As shown in Table 2, the presence of halloysite reduced the terminal relaxation time for both hydrogels with the crossover point. Specifically, we estimated a reduction of ca. 20% for the keratin/alginate hydrogel with $R_{K:A} = 1$, while the terminal relaxation time decreased by ca. 2 orders of magnitude for $R_{K:A} = 0.5$. On this basis, we can state that the effect of HNTs on the biopolymer crosslinking process is strongly more relevant for the hybrid hydrogel with the lower keratin amount. It is noteworthy that the addition of HNTs on the composite hydrogel with the lowest keratin content ($R_{K:A} = 0.25$) generated the greatest changes of the rheological characteristics being that crossing point was canceled out and the storage modulus became predominant to the loss modulus within the whole investigated ω range. According to the rheological data, we can conclude that the presence of HNTs favors the gelation process in the keratin/alginate hydrogels. Nevertheless, this effect is reduced by increasing the keratin content due to the specific interactions that occurs between the protein and the biopolymer. In this regard, it should be noted that literature reports that the addition of halloysite favored the formation of the network structure in the hydrogel based on pure alginate [13].

3.5 Hair treated by hydrogels: tensile performances and structure

Hydrogel systems (alginate, keratin/alginate and keratin/alginate filled with HNTs) were tested for the protective treatment of hair using the immersion protocol sketched in Figure 1. It should be noted that the $R_{K:A}$ was fixed at 1 for both composite hydrogels. The efficacy of the protection was investigated by studying the tensile properties of the treated hair samples after their exposure to UV irradiation for variable times (3 and 7 days). For comparison, DMA experiments were conducted on pristine hair. As shown in Figure 8, the stress vs strain curves of all hair samples present three consecutive characteristic regions: 1) linear increasing trend (elastic region); 2) a "plateau" with a slight increase of the stress on dependence of the strain (yield region); 3) enhancement of the slope of the stress vs strain profile up to the breaking (post-yield region). Similar trends were detected for human hair under different conditions in terms of temperature and relative humidity [69].

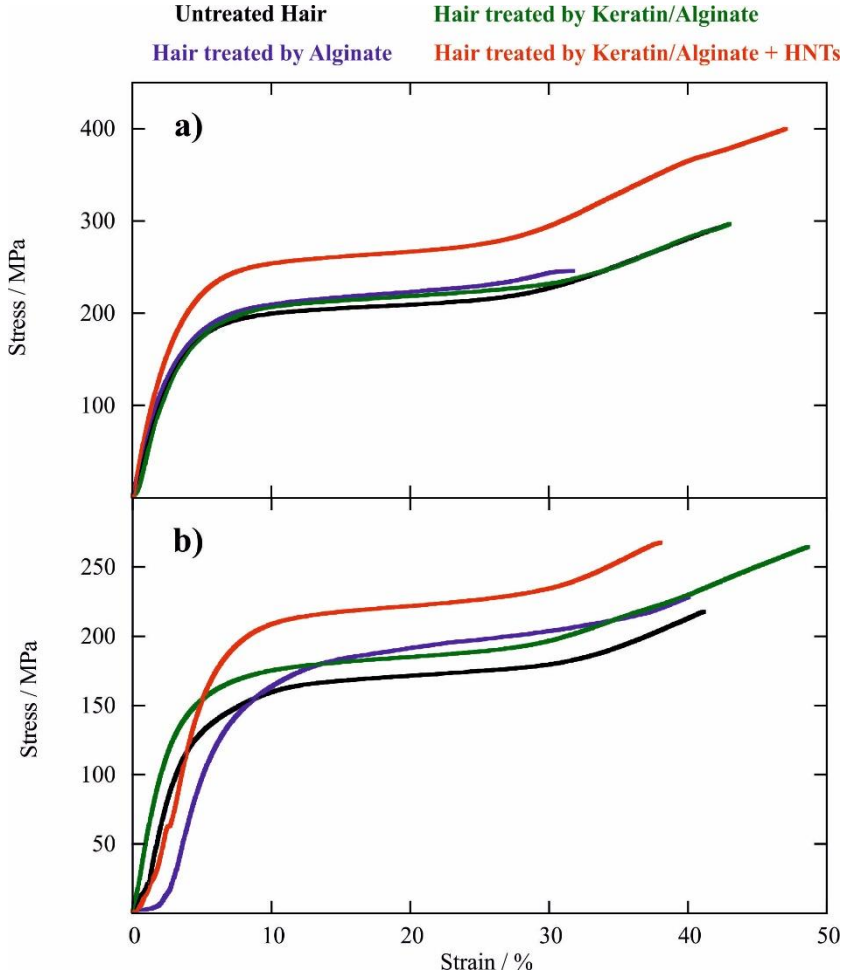

Fig. 8. Stress vs strain curves for untreated and treated hair samples exposed to UV irradiation for 3 (a) and 7 (b) days.

The analysis of the stress vs strain curves allowed us to determine several tensile properties related to the three mentioned regions. As concerns the elastic region, we calculated the Young modulus (Tables 3,4) from the slope of the stress vs strain trends. Within this, we detected that the treatment by keratin/alginate hydrogels induced enhancements of the Young modulus for the hair exposed to UV irradiation.

Table 3. Young modulus for untreated and treated hair samples exposed to UV irradiation for 3 days.

Sample	Young Modulus / MPa
Untreated hair	5540 ± 321
Hair treated by alginate hydrogel	5789 ± 315
Hair treated by keratin/alginate hydrogel	6202 ± 355
Hair treated by keratin/alginate/HNTs hydrogel	6607 ± 342

Table 4. Young modulus and ultimate elongation for untreated and treated hair samples exposed to UV irradiation for 7 days.

Sample	Young Modulus / MPa
Untreated hair	4289 ± 202
Hair treated by alginate hydrogel	3773 ± 230
Hair treated by keratin/alginate hydrogel	5380 ± 331
Hair treated by keratin/alginate/HNTs hydrogel	5001 ± 307

As concerns the hair samples aged for 3 days, we estimated that the treatment by unfilled keratin/alginate hydrogel induced an increase of ca. 12% for the Young modulus. Remarkably, a better improvement (ca. 19%) was achieved by adding halloysite nanotubes within the keratin/alginate hydrogel. Contrary to these results, the hair coating by pure alginate generated negligible variations on the Young modulus. Similarly to the Young modulus, the elongation at break (within the post-yield region) was enhanced by the hair treatment with the composite hydrogels. As concerns the hair exposed to UV irradiation for 3 days, we estimated the largest value (47.4 %) on the sample treated by keratin/alginate hydrogel filled with HNTs. After the UV exposure for a longer time (7 days), the treatment with unfilled keratin/alginate produced the hair with the highest elongation at break (48.6 %).

Moreover, we estimated the stress values at yield and breaking points (Figure 9). These parameters are crucial to evaluate the efficiency of the treatments because they provided direct information on the mechanical resistance of hair aged under UV irradiation.

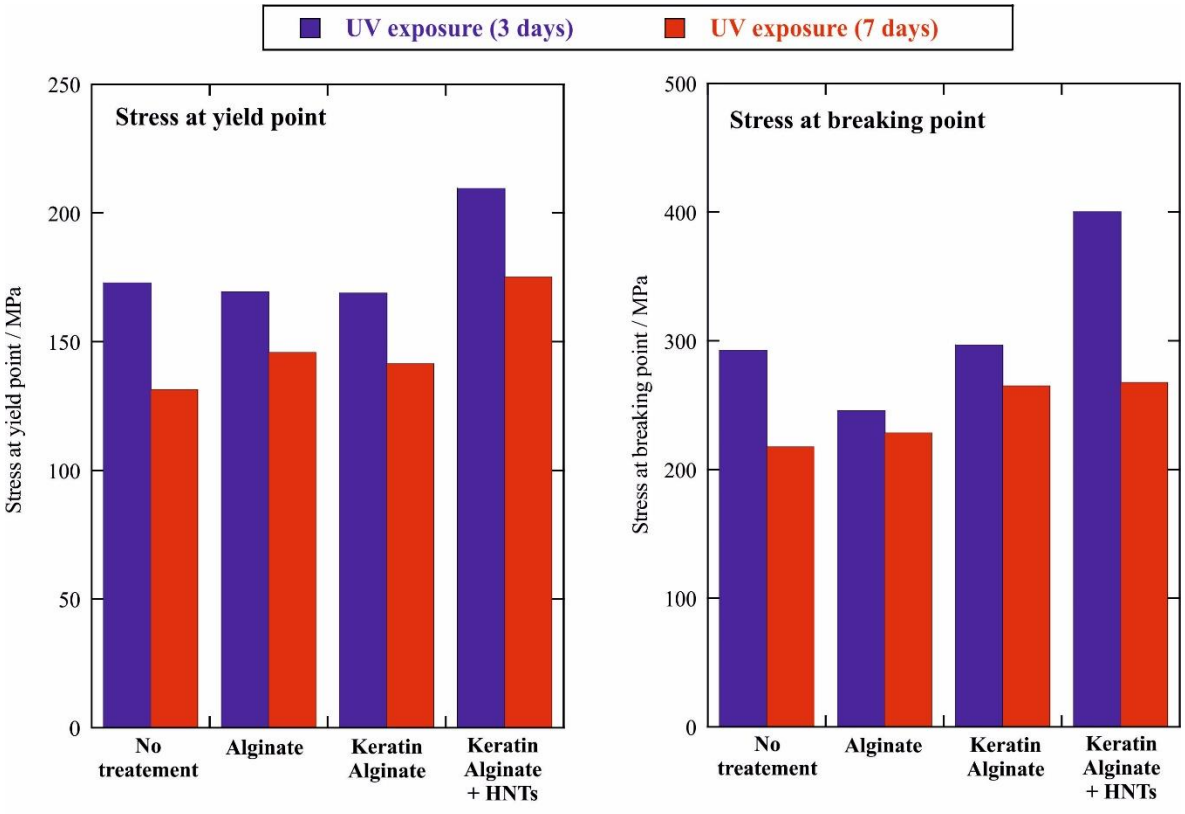

Fig. 9. Stress at yield point and stress at breaking point for untreated and treated hair samples after their exposure to UV irradiation for 3 and 7 days.

The stress at yield point is related to the transition from the elastic to the yield region, where structural changes of the hair occur because the α-helix coils can convert into β-sheets [70].

As shown in Figure 9, the hair treated with keratin/alginate/HNTs hydrogel possess the highest stress at yield point compared to the other samples. Regarding the hair aged for 3 days, we observed that the treatments by both alginate and keratin/alginate hydrogels do not determine variations on the stress at yield point, while we estimated an increase of ca. 21% after the coating through the composite hydrogel filled with HNTs. For a longer UV exposure (7 days), the hair coated with keratin/alginate/HNTs exhibited an enhancement of ca. 33% proving that the protection is extended over time. These observations are supported by the results on the stress at break (Figure 9), which showed that the hair treated by keratin/alginate/HNTs hydrogel possess the strongest mechanical resistance. Compared to the untreated hair samples, the coating by the HNTs filled hydrogel determined improvements equal to ca. 38% and 23% after UV aging of 3 and 7 days, respectively.

We observed that the treatment by unfilled keratin/alginate does not affect the stress at break for hair aged for 3 days, while an improvement of ca. 21% was detected after the UV exposure for 7 days. Furthermore, we calculated the stored energy up to breaking by the integration of the stress vs strain curves considering the specific sizes of the hair fibers. The obtained data are presented in Supplementary Material. After the UV exposure for 3 days, the hair treated by keratin/alginate/HNTs hydrogel exhibited the largest stored energy (132820 kJ m^{-3}) with an enhancement of 49% with respect to the untreated hair (89280 J m^{-3}). The effect of the hair coating on the capacity to store energy during the tensile experiments was attenuated by extending the UV irradiation to 7 days. We determined stored energy values of 67062 and 77240 kJ m^{-3} before and after the treatment with halloysite filled hydrogel, respectively.

As concerns the hair treated by keratin/alginate/HNTs hydrogel, we studied the effects of the thermal action produced by a commercial hair dryer on the tensile properties of UV aged fibers. The obtained results are reported in Supplementary Material (Table 5S). As a general result, we observed that the exposure to a flux of hot air slightly affect the mechanical performances of the fibers. This finding could be promising for the use of the keratin/alginate/halloysite hydrogel in shampoo formulations. For instance, the stress at breaking point was reduced by ca. 5% for the hair aged for 3 days. On the other hand, the thermal action of the hair dryer did not generate any significant variation on the hair aged by UV irradiation for 7 days being that the stresses at break are 268 ± 25 MPa and 266 ± 24 MPa before and after the exposure to the hot air flow, respectively.

Based on the tensile results, we can assert that the keratin/alginate/HNTs hydrogel is the most efficient as protective coating of hair fibers. The protection is due to both the deposition of keratin, which forms a UV shielding layer, and the adhesion of halloysite, which increases the light reflectivity of hair [44]. Namely, the addition of halloysite within the keratin/alginate hydrogel guarantees a stronger barrier effect that preserves the hair structure from the exposure to UV irradiation. This consideration is supported by SEM images of the treated hair samples (Figure 10), which evidenced the immobilization of the clay nanotubes on the cuticles.

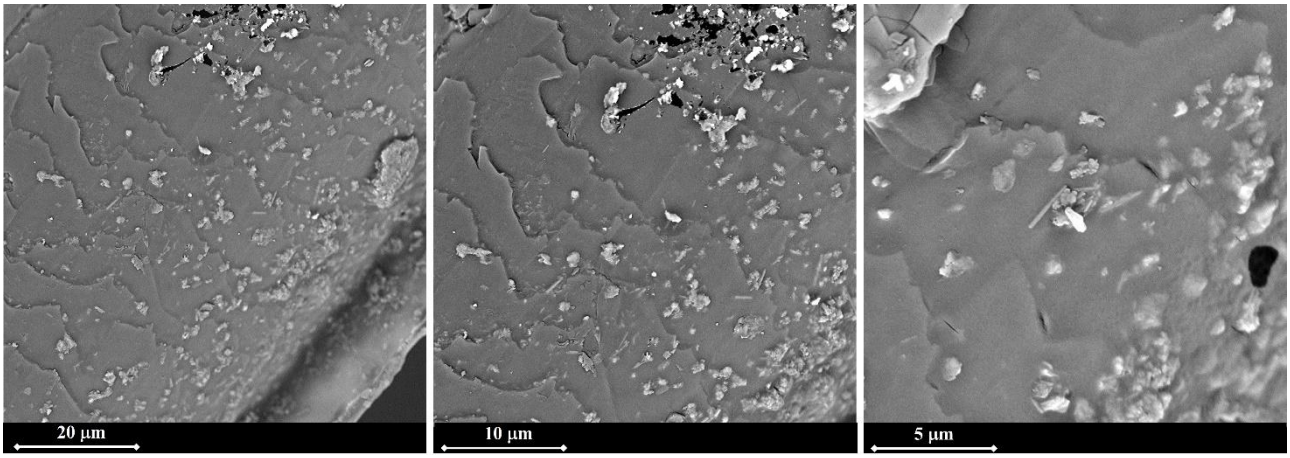

Fig. 10. SEM images of hair samples treated by keratin/alginate hydrogel filled with HNTs.

According to literature [44,45,48], the anchoring of HNTs protects the cuticles from the photo-damage and, consequently, the hair structure is slightly affected by the UV irradiation. The latter agrees with the previous observations on the mechanical characterization of the treated hair samples. In addition, SEM images showed a partial coating of the inter-cuticle spaces with the nanotubes randomly distributed and oriented. Similar observations were detected for hair treated by halloysite aqueous dispersions [45]. In conclusion, alginate/keratin hydrogel filled with HNTs acts as a UV protective coating layer that can be exploited for hair care formulations.

4. Conclusions

We proposed a novel protocol for the protective treatment of human hair based on the dipping procedure within keratin/alginate hydrogels containing halloysite nanotubes.

In order to determine the suitable conditions for an effective hair protective coating, preliminary investigations were conducted on keratin/alginate aqueous mixtures (before and after the halloysite addition) and their corresponding hydrogels, which were obtained by using Ca^{2+} ions as crosslinkers of the biopolymeric chains.

According to ζ potential results, we observed that supramolecular interactions occur between keratin and alginate dispersed in water at pH = 7 although both macromolecules are negatively charged. It should be noted that the keratin/alginate complexes can be confined within the positive inner surface of halloysite due to electrostatic attractions. It should be noted that the adsorption of keratin/alginate improved the aqueous colloidal stability of clay nanotubes due to the increase of their surface charge. In this regard, Dynamic Light Scattering (DLS) evidenced that the interactions with keratin/alginate complexes did not alter the diffusion of the nanotubes in water confirming the interpretation of the ζ potential data.

Then, we performed rheological measurements to explore the influence of keratin/alginate interactions and the subsequent filling with halloysite on the crosslinking of the biopolymeric chains. Based on the shear flow curves, we observed that the formation of the alginate network is not prevented. Remarkably, the shear thinning behavior of keratin/alginate composite hydrogel is enhanced by the filling with halloysite nanotubes. Frequency sweep experiments revealed that the viscoelastic properties of alginate hydrogel are significantly affected by the addition of both keratin and halloysite. Contrary to the pristine alginate, composite hydrogels showed a crossover point between storage and loss moduli trends highlighting that the biopolymer crosslinking in the hybrid systems is a reversible process. We detected that the increase of the keratin content generates a reduction of the terminal relaxation time in the composite hydrogels. This effect is largely enhanced by the filling with halloysite indicating that the nanotubes favor the formation of the network structure in the keratin/alginate gels.

Finally, we employed the hydrogel systems (alginate, keratin/alginate and keratin/alginate/halloysite) for the protective coating of human hair using an immersion procedure for 60 minutes. Their protection capacity was investigated by performing tensile tests on uncoated and coated hair fibers after their exposure to UV irradiation for different times. As a general result, we observed that the hair coated by keratin/alginate/halloysite hydrogel possess the greatest mechanical performances in terms of elasticity as well as strengths at yield and break points. Compared to untreated hair, we

estimated improvements of 38 and 23% for the breaking stress of samples aged for 3 and 7 days, respectively, evidencing that the hair protection is prolonged over time. It is important to evidence that the hair protection from photo-damage is related to the simultaneous presence of keratin and halloysite nanotubes, which adhere to the hair cuticles as visualized by SEM images.

On this basis, we can conclude that the keratin/alginate hydrogel filled with halloysite nanotubes is effective for the protective coating of human hair. Moreover, this work demonstrates that the rheological characteristics of alginate hydrogels can be controlled by the specific interactions with keratin as well as by the filling with halloysite. The attained knowledge can be helpful for designing novel formulations within biotechnological applications.

Acknowledgments.

The work was financially supported by FFR 2021 UFRDAC project and University of Palermo. The work of Rawil Fakhrullin was funded by Russian Science Foundation grant 20-13-00247.

References

[1] R. Chen, X. Xu, D. Yu, C. Xiao, M. Liu, J. Huang, T. Mao, C. Zheng, Z. Wang, X. Wu, Highly stretchable and fatigue resistant hydrogels with low Young's modulus as transparent and flexible strain sensors, J Mater Chem C. 6 (2018) 11193–11201. https://doi.org/10.1039/C8TC02583E.

[2] H. Ding, X. Liang, Q. Wang, M. Wang, Z. Li, G. Sun, A semi-interpenetrating network ionic composite hydrogel with low modulus, fast self-recoverability and high conductivity as flexible sensor, Carbohydr. Polym. 248 (2020) 116797. https://doi.org/10.1016/j.carbpol.2020.116797.

[3] Z. Sun, Y. Hu, C. Wei, R. Hao, C. Hao, W. Liu, H. Liu, M. Huang, S. He, M. Yang, Transparent, photothermal and stretchable alginate-based hydrogels for remote actuation and human motion sensing, Carbohydr. Polym. 293 (2022) 119727. https://doi.org/10.1016/j.carbpol.2022.119727.

[4] S. Naahidi, M. Jafari, M. Logan, Y. Wang, Y. Yuan, H. Bae, B. Dixon, P. Chen, Biocompatibility of hydrogel-based scaffolds for tissue engineering applications, Biotechnol. Adv. 35 (2017) 530–544. https://doi.org/10.1016/j.biotechadv.2017.05.006.

[5] R. Silva, R. Singh, B. Sarker, D.G. Papageorgiou, J.A. Juhasz, J.A. Roether, I. Cicha, J. Kaschta, D.W. Schubert, K. Chrissafis, R. Detsch, A.R. Boccaccini, Hybrid hydrogels based on keratin and alginate for tissue engineering, J Mater Chem B. 2 (2014) 5441–5451. https://doi.org/10.1039/C4TB00776J.

[6] C. Luo, M. Huang, X. Sun, N. Wei, H. Shi, H. Li, M. Lin, J. Sun, Super-Strong, Nonswellable, and Biocompatible Hydrogels Inspired by Human Tendons, ACS Appl. Mater. Interfaces. 14 (2022) 2638–2649. https://doi.org/10.1021/acsami.1c23102.
[7] L. Ma, Y. Tan, X. Chen, Y. Ran, Q. Tong, L. Tang, W. Su, X. Wang, X. Li, Injectable oxidized alginate/carboxylmethyl chitosan hydrogels functionalized with nanoparticles for wound repair, Carbohydr. Polym. 293 (2022) 119733. https://doi.org/10.1016/j.carbpol.2022.119733.
[8] S.M. Hashemnejad, S. Kundu, Rheological properties and failure of alginate hydrogels with ionic and covalent crosslinks, Soft Matter. 15 (2019) 7852–7862. https://doi.org/10.1039/C9SM01039D.
[9] P. Agulhon, M. Robitzer, J.-P. Habas, F. Quignard, Influence of both cation and alginate nature on the rheological behavior of transition metal alginate gels, Carbohydr. Polym. 112 (2014) 525–531. https://doi.org/10.1016/j.carbpol.2014.05.097.
[10] M.I. Neves, L. Moroni, C.C. Barrias, Modulating Alginate Hydrogels for Improved Biological Performance as Cellular 3D Microenvironments, Front. Bioeng. Biotechnol. 8 (2020). https://doi.org/10.3389/fbioe.2020.00665.
[11] M.H. Kim, Y.W. Lee, W.-K. Jung, J. Oh, S.Y. Nam, Enhanced rheological behaviors of alginate hydrogels with carrageenan for extrusion-based bioprinting, J. Mech. Behav. Biomed. Mater. 98 (2019) 187–194. https://doi.org/10.1016/j.jmbbm.2019.06.014.
[12] A.A. Aldana, F. Valente, R. Dilley, B. Doyle, Development of 3D bioprinted GelMA-alginate hydrogels with tunable mechanical properties, Bioprinting. 21 (2021) e00105. https://doi.org/10.1016/j.bprint.2020.e00105.
[13] S.A. Glukhova, V.S. Molchanov, B.V. Lokshin, A.V. Rogachev, A.A. Tsarenko, T.D. Patsaev, R.A. Kamyshinsky, O.E. Philippova, Printable Alginate Hydrogels with Embedded Network of Halloysite Nanotubes: Effect of Polymer Cross-Linking on Rheological Properties and Microstructure, Polymers. 13 (2021). https://doi.org/10.3390/polym13234130.
[14] Y. Jin, C. Liu, W. Chai, A. Compaan, Y. Huang, Self-Supporting Nanoclay as Internal Scaffold Material for Direct Printing of Soft Hydrogel Composite Structures in Air, ACS Appl. Mater. Interfaces. 9 (2017) 17456–17465. https://doi.org/10.1021/acsami.7b03613.
[15] K. Markstedt, A. Mantas, I. Tournier, H. Martínez Ávila, D. Hägg, P. Gatenholm, 3D Bioprinting Human Chondrocytes with Nanocellulose–Alginate Bioink for Cartilage Tissue Engineering Applications, Biomacromolecules. 16 (2015) 1489–1496. https://doi.org/10.1021/acs.biomac.5b00188.
[16] L.K. Narayanan, P. Huebner, M.B. Fisher, J.T. Spang, B. Starly, R.A. Shirwaiker, 3D-Bioprinting of Polylactic Acid (PLA) Nanofiber–Alginate Hydrogel Bioink Containing Human Adipose-Derived Stem Cells, ACS Biomater. Sci. Eng. 2 (2016) 1732–1742. https://doi.org/10.1021/acsbiomaterials.6b00196.
[17] G. Cavallaro, L. Lisuzzo, G. Lazzara, S. Milioto, Printable Hydrogels Based on Alginate and Halloysite Nanotubes, Int. J. Mol. Sci. 23 (2022). https://doi.org/10.3390/ijms23063294.
[18] B. Huang, M. Liu, Z. Long, Y. Shen, C. Zhou, Effects of halloysite nanotubes on physical properties and cytocompatibility of alginate composite hydrogels, Mater. Sci. Eng. C. 70 (2017) 303–310. https://doi.org/10.1016/j.msec.2016.09.001.
[19] Q. Liu, Q. Li, S. Xu, Q. Zheng, X. Cao, Preparation and Properties of 3D Printed Alginate–Chitosan Polyion Complex Hydrogels for Tissue Engineering, Polymers. 10 (2018). https://doi.org/10.3390/polym10060664.
[20] M. Zhang, T. Qian, Z. Deng, F. Hang, 3D printed double-network alginate hydrogels containing polyphosphate for bioenergetics and bone regeneration, Int. J. Biol. Macromol. 188 (2021) 639–648. https://doi.org/10.1016/j.ijbiomac.2021.08.066.
[21] M.D. Di Giuseppe, N. Law, B. Webb, R.A. Macrae, L.J. Liew, T.B. Sercombe, R.J. Dilley, B.J. Doyle, Mechanical behaviour of alginate-gelatin hydrogels for 3D bioprinting, J. Mech. Behav. Biomed. Mater. 79 (2018) 150–157. https://doi.org/10.1016/j.jmbbm.2017.12.018.

[22] Y. Hu, S. Hu, S. Zhang, S. Dong, J. Hu, L. Kang, X. Yang, A double-layer hydrogel based on alginate-carboxymethyl cellulose and synthetic polymer as sustained drug delivery system, Sci. Rep. 11 (2021) 9142. https://doi.org/10.1038/s41598-021-88503-1.
[23] E.G. Arafa, M.W. Sabaa, R.R. Mohamed, E.M. Kamel, A.M. Elzanaty, A.M. Mahmoud, O.F. Abdel-Gawad, Eco-friendly and biodegradable sodium alginate/quaternized chitosan hydrogel for controlled release of urea and its antimicrobial activity, Carbohydr. Polym. 291 (2022) 119555. https://doi.org/10.1016/j.carbpol.2022.119555.
[24] F. Shuai, Y. Zhang, Y. Yin, H. Zhao, X. Han, Fabrication of an injectable iron (III) crosslinked alginate-hyaluronic acid hydrogel with shear-thinning and antimicrobial activities, Carbohydr. Polym. 260 (2021) 117777. https://doi.org/10.1016/j.carbpol.2021.117777.
[25] A.C. Hernández-González, L. Téllez-Jurado, L.M. Rodríguez-Lorenzo, Alginate hydrogels for bone tissue engineering, from injectables to bioprinting: A review, Carbohydr. Polym. 229 (2020) 115514. https://doi.org/10.1016/j.carbpol.2019.115514.
[26] S. Balaji, R. Kumar, R. Sripriya, U. Rao, A. Mandal, P. Kakkar, P.N. Reddy, P.K. Sehgal, Characterization of keratin–collagen 3D scaffold for biomedical applications, Polym. Adv. Technol. 23 (2012) 500–507. https://doi.org/10.1002/pat.1905.
[27] C. Popescu, H. Höcker, Hair—the most sophisticated biological composite material, Chem Soc Rev. 36 (2007) 1282–1291. https://doi.org/10.1039/B604537P.
[28] Z.K. Moay, L.T.H. Nguyen, P. Hartrianti, D.P. Lunny, D. Leavesley, Y.O. Kok, S.J. Chong, A.W.C. Chua, S.-I. Tee, K.W. Ng, Keratin-Alginate Sponges Support Healing of Partial-Thickness Burns, Int. J. Mol. Sci. 22 (2021). https://doi.org/10.3390/ijms22168594.
[29] V. Bertolino, G. Cavallaro, S. Milioto, G. Lazzara, Polysaccharides/Halloysite nanotubes for smart bionanocomposite materials, Carbohydr. Polym. 245 (2020) 116502. https://doi.org/10.1016/j.carbpol.2020.116502.
[30] G. Biddeci, G. Cavallaro, F. Di Blasi, G. Lazzara, M. Massaro, S. Milioto, F. Parisi, S. Riela, G. Spinelli, Halloysite nanotubes loaded with peppermint essential oil as filler for functional biopolymer film, Carbohydr. Polym. 152 (2016) 548–557. https://doi.org/10.1016/j.carbpol.2016.07.041.
[31] E. Boccalon, P. Sassi, L. Pioppi, A. Ricci, M. Marinozzi, G. Gorrasi, M. Nocchetti, Onion skin extract immobilized on Halloysite-layered double hydroxide filler as active pH indicator for food packaging, Appl. Clay Sci. 227 (2022) 106592. https://doi.org/10.1016/j.clay.2022.106592.
[32] G. Gorrasi, Dispersion of halloysite loaded with natural antimicrobials into pectins: Characterization and controlled release analysis, Carbohydr. Polym. 127 (2015) 47–53. https://doi.org/10.1016/j.carbpol.2015.03.050.
[33] K. Govindasamy, N.A. Dahlan, P. Janarthanan, K.L. Goh, S.-P. Chai, P. Pasbakhsh, Electrospun chitosan/polyethylene-oxide (PEO)/halloysites (HAL) membranes for bone regeneration applications, Appl. Clay Sci. 190 (2020) 105601. https://doi.org/10.1016/j.clay.2020.105601.
[34] O. Owoseni, Y. Su, S. Raghavan, A. Bose, V.T. John, Hydrophobically modified chitosan biopolymer connects halloysite nanotubes at the oil-water interface as complementary pair for stabilizing oil droplets, J. Colloid Interface Sci. 620 (2022) 135–143. https://doi.org/10.1016/j.jcis.2022.03.142.
[35] Y. Su, Y. Zhang, H. Ke, G. McPherson, J. He, X. Zhang, V.T. John, Environmental Remediation of Chlorinated Hydrocarbons Using Biopolymer Stabilized Iron Loaded Halloysite Nanotubes, ACS Sustain. Chem. Eng. 5 (2017) 10976–10985. https://doi.org/10.1021/acssuschemeng.7b02872.
[36] M. Fizir, P. Dramou, N.S. Dahiru, W. Ruya, T. Huang, H. He, Halloysite nanotubes in analytical sciences and in drug delivery: A review, Microchim. Acta. 185 (2018) 389. https://doi.org/10.1007/s00604-018-2908-1.

[37] I.A. Iakovlev, A.Y. Deviatov, Y. Lvov, G. Fakhrullina, R.F. Fakhrullin, V.V. Mazurenko, Probing Diffusive Dynamics of Natural Tubule Nanoclays with Machine Learning, ACS Nano. 16 (2022) 5867–5873. https://doi.org/10.1021/acsnano.1c11025.
[38] L. Lisuzzo, G. Cavallaro, P. Pasbakhsh, S. Milioto, G. Lazzara, Why does vacuum drive to the loading of halloysite nanotubes? The key role of water confinement, J. Colloid Interface Sci. 547 (2019) 361–369. https://doi.org/10.1016/j.jcis.2019.04.012.
[39] A.C. Santos, I. Pereira, S. Reis, F. Veiga, M. Saleh, Y. Lvov, Biomedical potential of clay nanotube formulations and their toxicity assessment, Expert Opin. Drug Deliv. 16 (2019) 1169–1182. https://doi.org/10.1080/17425247.2019.1665020.
[40] Y.-P. Wu, J. Yang, H.-Y. Gao, Y. Shen, L. Jiang, C. Zhou, Y.-F. Li, R.-R. He, M. Liu, Folate-Conjugated Halloysite Nanotubes, an Efficient Drug Carrier, Deliver Doxorubicin for Targeted Therapy of Breast Cancer, ACS Appl. Nano Mater. 1 (2018) 595–608. https://doi.org/10.1021/acsanm.7b00087.
[41] M. Liu, C. Wu, Y. Jiao, S. Xiong, C. Zhou, Chitosan-halloysite nanotubes nanocomposite scaffolds for tissue engineering, J. Mater. Chem. B. 1 (2013) 2078–2089. https://doi.org/10.1039/C3TB20084A.
[42] M. Liu, L. Dai, H. Shi, S. Xiong, C. Zhou, In vitro evaluation of alginate/halloysite nanotube composite scaffolds for tissue engineering, Mater. Sci. Eng. C. 49 (2015) 700–712. https://doi.org/10.1016/j.msec.2015.01.037.
[43] S.S. Suner, S. Demirci, B. Yetiskin, R. Fakhrullin, E. Naumenko, O. Okay, R.S. Ayyala, N. Sahiner, Cryogel composites based on hyaluronic acid and halloysite nanotubes as scaffold for tissue engineering, Int. J. Biol. Macromol. 130 (2019) 627–635. https://doi.org/10.1016/j.ijbiomac.2019.03.025.
[44] G. Cavallaro, S. Milioto, S. Konnova, G. Fakhrullina, F. Akhatova, G. Lazzara, R. Fakhrullin, Y. Lvov, Halloysite/Keratin Nanocomposite for Human Hair Photoprotection Coating, ACS Appl. Mater. Interfaces. 12 (2020) 24348–24362. https://doi.org/10.1021/acsami.0c05252.
[45] A. Panchal, G. Fakhrullina, R. Fakhrullin, Y. Lvov, Self-assembly of clay nanotubes on hair surface for medical and cosmetic formulations, Nanoscale. 10 (2018) 18205–18216. https://doi.org/10.1039/C8NR05949G.
[46] N. Rahman, F.H. Scott, Y. Lvov, A. Stavitskaya, F. Akhatova, S. Konnova, G. Fakhrullina, R. Fakhrullin, Clay Nanotube Immobilization on Animal Hair for Sustained Anti-Lice Protection, Pharmaceutics. 13 (2021). https://doi.org/10.3390/pharmaceutics13091477.
[47] N. Rahman, A. Karan, Y. Lvov, Z. Liao, A. Parekh, R. Rughani, S. Muthukrishnan, Lawsone and Indigo-Loaded Sepiolite Nanofibers for Hair Coloring with Sustained Release, ACS Appl. Nano Mater. 5 (2022) 1855–1863. https://doi.org/10.1021/acsanm.1c03472.
[48] A.C. Santos, A. Panchal, N. Rahman, M. Pereira-Silva, I. Pereira, F. Veiga, Y. Lvov, Evolution of Hair Treatment and Care: Prospects of Nanotube-Based Formulations, Nanomaterials. 9 (2019). https://doi.org/10.3390/nano9060903.
[49] A. Glotov, A. Vutolkina, A. Pimerzin, V. Vinokurov, Y. Lvov, Clay nanotube-metal core/shell catalysts for hydroprocesses, Chem Soc Rev. 50 (2021) 9240–9277. https://doi.org/10.1039/D1CS00502B.
[50] L. Lisuzzo, G. Cavallaro, S. Milioto, G. Lazzara, Halloysite nanotubes as nanoreactors for heterogeneous micellar catalysis, J. Colloid Interface Sci. 608 (2022) 424–434. https://doi.org/10.1016/j.jcis.2021.09.146.
[51] F. Liu, L. Bai, H. Zhang, H. Song, L. Hu, Y. Wu, X. Ba, Smart H2O2-Responsive Drug Delivery System Made by Halloysite Nanotubes and Carbohydrate Polymers, ACS Appl. Mater. Interfaces. 9 (2017) 31626–31633. https://doi.org/10.1021/acsami.7b10867.
[52] Y. Liu, H. Guan, J. Zhang, Y. Zhao, J.-H. Yang, B. Zhang, Polydopamine-coated halloysite nanotubes supported AgPd nanoalloy: An efficient catalyst for hydrolysis of ammonia borane, Int. J. Hydrog. Energy. 43 (2018) 2754–2762. https://doi.org/10.1016/j.ijhydene.2017.12.105.

[53] Y. Liu, J. Zhang, H. Guan, Y. Zhao, J.-H. Yang, B. Zhang, Preparation of bimetallic Cu-Co nanocatalysts on poly (diallyldimethylammonium chloride) functionalized halloysite nanotubes for hydrolytic dehydrogenation of ammonia borane, Appl. Surf. Sci. 427 (2018) 106–113. https://doi.org/10.1016/j.apsusc.2017.08.171.
[54] S. Sadjadi, M.M. Heravi, M. Malmir, Pd@HNTs-CDNS-g-C3N4: A novel heterogeneous catalyst for promoting ligand and copper-free Sonogashira and Heck coupling reactions, benefits from halloysite and cyclodextrin chemistry and g-C3N4 contribution to suppress Pd leaching, Carbohydr. Polym. 186 (2018) 25–34. https://doi.org/10.1016/j.carbpol.2018.01.023.
[55] S. Sadjadi, G. Lazzara, M. Malmir, M.M. Heravi, Pd nanoparticles immobilized on the poly-dopamine decorated halloysite nanotubes hybridized with N-doped porous carbon monolayer: A versatile catalyst for promoting Pd catalyzed reactions, J. Catal. 366 (2018) 245–257. https://doi.org/10.1016/j.jcat.2018.08.013.
[56] B. Tang, H. Zhang, C. Cheng, H. Jiang, L. Bai, X. Ba, Y. Wu, Development of halloysite nanotube-based hydrogel with colorimetric H2O2-responsive character, Appl. Clay Sci. 212 (2021) 106230. https://doi.org/10.1016/j.clay.2021.106230.
[57] J. Tully, R. Yendluri, Y. Lvov, Halloysite Clay Nanotubes for Enzyme Immobilization, Biomacromolecules. 17 (2016) 615–621. https://doi.org/10.1021/acs.biomac.5b01542.
[58] C. Chao, H. Guan, J. Zhang, Y. Liu, Y. Zhao, B. Zhang, Immobilization of laccase onto porous polyvinyl alcohol/halloysite hybrid beads for dye removal, Water Sci. Technol. 77 (2017) 809–818. https://doi.org/10.2166/wst.2017.594.
[59] C. Duce, V.D. Porta, E. Bramanti, B. Campanella, A. Spepi, M.R. Tiné, Loading of halloysite nanotubes with BSA, α -Lac and β -Lg: a Fourier transform infrared spectroscopic and thermogravimetric study, Nanotechnology. 28 (2017) 055706.
[60] N. Siva Gangi Reddy, K. Madhusudana Rao, S.Y. Park, T. Kim, I. Chung, Fabrication of Aminosilanized Halloysite Based Floating Biopolymer Composites for Sustained Gastro Retentive Release of Curcumin, Macromol. Res. 27 (2019) 490–496. https://doi.org/10.1007/s13233-019-7062-z.
[61] A. Pietraszek, A. Karewicz, M. Widnic, D. Lachowicz, M. Gajewska, A. Bernasik, M. Nowakowska, Halloysite-alkaline phosphatase system—A potential bioactive component of scaffold for bone tissue engineering, Colloids Surf. B Biointerfaces. 173 (2019) 1–8. https://doi.org/10.1016/j.colsurfb.2018.09.040.
[62] F. Abasalizadeh, S.V. Moghaddam, E. Alizadeh, E. akbari, E. Kashani, S.M.B. Fazljou, M. Torbati, A. Akbarzadeh, Alginate-based hydrogels as drug delivery vehicles in cancer treatment and their applications in wound dressing and 3D bioprinting, J. Biol. Eng. 14 (2020) 8. https://doi.org/10.1186/s13036-020-0227-7.
[63] J. Ma, Y. Lin, X. Chen, B. Zhao, J. Zhang, Flow behavior, thixotropy and dynamical viscoelasticity of sodium alginate aqueous solutions, Food Hydrocoll. 38 (2014) 119–128. https://doi.org/10.1016/j.foodhyd.2013.11.016.
[64] C. Su, Y. Feng, J. Ye, Y. Zhang, Z. Gao, M. Zhao, N. Yang, K. Nishinari, Y. Fang, Effect of sodium alginate on the stability of natural soybean oil body emulsions, RSC Adv. 8 (2018) 4731–4741. https://doi.org/10.1039/C7RA09375F.
[65] G. Lazzara, G. Cavallaro, A. Panchal, R. Fakhrullin, A. Stavitskaya, V. Vinokurov, Y. Lvov, An assembly of organic-inorganic composites using halloysite clay nanotubes, Curr. Opin. Colloid Interface Sci. 35 (2018) 42–50. https://doi.org/10.1016/j.cocis.2018.01.002.
[66] M. Blanco-López, Á. González-Garcinuño, A. Tabernero, E.M. Martín del Valle, Steady and Oscillatory Shear Flow Behavior of Different Polysaccharides with Laponite®, Polymers. 13 (2021). https://doi.org/10.3390/polym13060966.
[67] C. Rodríguez-Rivero, L. Hilliou, E.M. Martín del Valle, M.A. Galán, Rheological characterization of commercial highly viscous alginate solutions in shear and extensional flows, Rheol. Acta. 53 (2014) 559–570. https://doi.org/10.1007/s00397-014-0780-4.

[68] J. Zlopasa, B. Norder, E.A.B. Koenders, S.J. Picken, Rheological investigation of specific interactions in Na Alginate and Na MMT suspension, Carbohydr. Polym. 151 (2016) 144–149. https://doi.org/10.1016/j.carbpol.2016.05.055.
[69] Y. Yu, W. Yang, B. Wang, M.A. Meyers, Structure and mechanical behavior of human hair, Mater. Sci. Eng. C. 73 (2017) 152–163. https://doi.org/10.1016/j.msec.2016.12.008.
[70] L. Kreplak, J. Doucet, P. Dumas, F. Briki, New Aspects of the α-Helix to β-Sheet Transition in Stretched Hard α-Keratin Fibers, Biophys. J. 87 (2004) 640–647. https://doi.org/10.1529/biophysj.103.036749.

Graphical Abstract